

Basal forebrain atrophy and cortical amyloid deposition in nondemented elderly subjects

Michel J. Grothe^{a,*}, Michael Ewers^b, Bernd Krause^c, Helmut Heinsen^d, Stefan J. Teipel^{a,e},
for the Alzheimer's Disease Neuroimaging Initiative¹

^aGerman Center for Neurodegenerative Diseases (DZNE), Rostock, Germany

^bInstitute for Stroke and Dementia Research, Klinikum Grosshadern, Ludwig-Maximilians University, Munich, Germany

^cDepartment of Nuclear Medicine, University of Rostock, Rostock, Germany

^dLaboratory of Morphological Brain Research, Department of Psychiatry, University of Würzburg, Würzburg, Germany

^eDepartment of Psychosomatic Medicine, University of Rostock, Rostock, Germany

Abstract

Background: Both neurodegeneration of the cholinergic basal forebrain (BF) and deposition of β -amyloid are early events in the course of Alzheimer's disease (AD). Associations between increased amyloid pathology and cholinergic atrophy have been described in autopsy studies.

Methods: We used structural MRI and AV45-PET amyloid imaging data of 225 cognitively normal or mildly impaired elderly subjects from the Alzheimer's Disease Neuroimaging Initiative to assess in vivo associations between BF atrophy and cortical amyloid deposition. Associations were examined using region-of-interest (ROI) and voxel-based approaches with reference to cytoarchitectonic mappings of the cholinergic BF nuclei.

Results: ROI- and voxel-based approaches yielded complementary evidence for an association between BF volume and cortical amyloid deposition in presymptomatic and prodementia stages of AD, irrespective of age, gender, and *APOE* genotype.

Conclusions: The observed correlations between BF atrophy and cortical amyloid load likely reflect associations between cholinergic degeneration and amyloid pathology as reported in neuropathologic examination studies.

© 2014 The Alzheimer's Association. All rights reserved.

Keywords:

Alzheimer's disease; Mild cognitive impairment; Preclinical; Prodementia; AV45-PET; Amyloid; MRI; Voxel-based; Cytoarchitectonic; Cholinergic basal forebrain; Substantia innominata; Nucleus basalis Meynert

1. Introduction

Cholinergic neurons of the basal forebrain (BF) provide the cholinergic innervation of the entire cortical mantle [1]. In normal aging these neurons are known to

undergo moderate neurodegenerative changes, whereas Alzheimer's disease (AD) is characterized by severe cholinergic neuron loss and cortical cholinergic denervation [2–5].

The cholinergic deficit in AD does not arise in isolation. Cerebral amyloid deposition, as caused by altered processing of the membrane-bound amyloid precursor protein (APP), is widely considered to be a primary etiologic factor in AD. Thus, the amyloid cascade model proposes a sequence of pathologic events in AD that begins with cerebral amyloid deposition several years to decades before the first symptoms appear. Over the years, the primary amyloid-related molecular pathology initiates downstream pathologic events, such as the formation of intracellular

¹Data used in the preparation of this article were obtained from the Alzheimer's Disease Neuroimaging Initiative (ADNI) database (<http://adni.loni.usc.edu/>). As such, the investigators within the ADNI contributed to the design and implementation and/or provided data but did not participate in analysis or writing of this report. A complete listing of ADNI investigators can be found at: <http://adni.loni.usc.edu/about/centers-cores/study-sites/>.

*Corresponding author. Tel.: 01149-381-494-9479; Fax: 01149-381-494-9472.

E-mail address: michel@grothe.org

neurofibrillary tangles, which ultimately lead to neuronal dysfunction, atrophy, and cognitive decline [6].

An increasing body of evidence suggests that amyloid accumulation and cholinergic dysfunction are tightly interrelated and may mutually influence each other [7]. Transgenic animal models of amyloid pathology develop alterations of the cholinergic system [8] and cortical cholinergic denervation leads to increased amyloid deposition in wild-type animals [9]. Histopathologic studies on the relationship between amyloid deposition and cholinergic decline in AD brain specimens showed that increased cortical amyloid load was associated with degeneration of cholinergic BF neurons [10,11] and reduced cortical choline acetyltransferase (ChAT) activity [4,12]. Similar findings were observed in autopsies from nondemented elderly subjects showing evidence of AD pathology [13,14], but so far there is no *in vivo* evidence for a relationship between cholinergic degeneration and increased amyloid deposition in humans.

In the present study, we combined novel amyloid-sensitive positron emission tomography (AV45-PET) [15] with morphometric analysis of structural magnetic resonance imaging (MRI) scans guided by cytoarchitectonic maps of the BF cholinergic nuclei [16–19] to assess the relationship between cortical amyloid deposition and BF atrophy in a large sample of nondemented subjects from the Alzheimer's Disease Neuroimaging Initiative (ADNI).

2. Methods

Data used in the preparation of this article were obtained from the ADNI database (<http://adni.loni.usc.edu/>). The ADNI was launched in 2003 with the primary goal of testing whether neuroimaging, neuropsychologic, and other biologic measurements can be used as reliable *in vivo* markers of AD pathogenesis. A fuller description of ADNI and up-to-date information is available at www.adni-info.org.

2.1. Subjects

AV45-PET and structural MRI scans were retrieved from the ADNI-GO/-2 extensions of the ADNI project and included imaging data of 57 cognitively normal (CN) elderly subjects, 156 subjects with early-stage mild cognitive impairment (EMCI), and 32 subjects in a more advanced stage of MCI (LMCI). Detailed inclusion criteria for the diagnostic categories can be found at the ADNI website (<http://adni.loni.usc.edu/methods/>). Briefly, CN subjects are those with: MMSE scores of between 24 and 30 (inclusive); a CDR of 0; no depression; no MCI; and no dementia. EMCI subjects are those with: MMSE scores between 24 and 30 (inclusive); a subjective memory concern reported by subject, informant, or clinician; objective memory loss as measured by education-adjusted scores on delayed recall (Wechsler Memory Scale Logical Memory II); a CDR of 0.5; absence of significant levels of impairment in other cognitive domains; essentially preserved activities

of daily living; and an absence of dementia. Diagnosis of LMCI differs from that of EMCI only with regard to a higher degree of impairment according to the logical memory test.

2.2. Imaging data acquisition

ADNI-GO/-2 MRI data were acquired on multiple 3-T MRI scanners using scanner-specific T1-weighted sagittal 3D MPRAGE sequences. To increase signal uniformity across the multicenter scanner platforms, original MPRAGE acquisitions in ADNI undergo standardized image preprocessing correction steps.

AV45-PET data were acquired on multiple instruments of varying resolution and following different platform-specific acquisition protocols. Similar to the MRI data, PET data in ADNI undergo standardized image preprocessing correction steps aimed at increasing data uniformity across the multicenter acquisitions.

More detailed information on the different imaging protocols employed across ADNI sites and standardized image preprocessing steps for MRI and PET acquisitions can be found on the ADNI website (<http://adni.loni.usc.edu/methods/>).

2.3. MRI processing

Imaging data were processed using SPM8 (Wellcome Trust Center for Neuroimaging) implemented in MATLAB R2007a (The MathWorks, Natick, MA). MRI scans were automatically segmented into gray-matter (GM), white-matter (WM), and cerebrospinal fluid (CSF) partitions using the segmentation routine of the VBM8 toolbox (<http://dbm.neuro.uni-jena.de/vbm/>). The GM partitions were then high-dimensionally warped [20] to an aging/AD-specific reference template, based on a previous study [18]. Voxel values were modulated for volumetric changes, and for voxel-based analyses modulated warped GM segments were smoothed with a Gaussian smoothing kernel of 8-mm full-width at half-maximum (FWHM). All preprocessed GM maps passed a visual inspection for overall segmentation and registration accuracy.

Individual GM volumes of regions-of-interest (ROIs) were extracted automatically from the warped GM segments by summing up the modulated GM voxel values within the respective ROI masks in the reference space (see later). For further analyses, extracted regional GM volumes were divided by the total intracranial volume (TIV), calculated as the sum of total volumes of the GM, WM, and CSF partitions.

2.4. Definition of BF and hippocampus ROIs

According to Mesulam's nomenclature [1], the cholinergic BF is composed of four groups of cholinergic cells, which correspond to the medial septum (Ch1), the vertical and horizontal limb of the diagonal band of Broca (Ch2 and Ch3), and the nucleus basalis Meynert (NBM, Ch4).

The cholinergic nuclei lack clear anatomic borders that could be easily identified on MRI scans, rendering manual delineation impractical. The BF mask used in this study was therefore based on a cytoarchitectonic map of BF cholinergic nuclei [16], which was nonlinearly registered to the aging/AD-specific reference template (Fig. 1). Voxel-based results were further compared with previously published center-of-gravity coordinates of cholinergic BF nuclei based on probabilistic cytoarchitectonic maps [21].

For comparison, we also examined associations between amyloid deposition and hippocampus volume as it is the best-studied volumetric MRI marker of early AD-related GM atrophy [22]. The ROI mask was obtained by manual delineation of the hippocampus in the reference template using the interactive software Display (<http://www.bic.mni.mcgill.ca/ServicesSoftwareVisualization/Display>), and a previously described protocol for segmentation of the medial temporal lobe [23].

2.5. PET processing

Cortical AV45 standardized uptake value ratios (SUVRs) relative to cerebellar GM uptake were calculated by one of the ADNI PET core laboratories and are available on the ADNI server. Amyloid positivity (+) or negativity (–) was established based on this cortex-to-cerebellar GM SUVR using a recommended cut-off of 1.28 [24]. More detailed information on PET processing, SUVR calculation, and cut-off selection can be found on the ADNI website (<http://adni.loni.usc.edu/methods/pet-analysis/>).

To examine associations between BF volume and regional AV45 uptake on a voxel level, we also processed the AV45 scans using SPM-based processing routines. Each subject's AV45 scan was rigidly coregistered to the corresponding structural MRI scan and warped to the aging/AD-specific reference space using the deformation fields derived from the registration of the MRI scans. To limit signal spillover from surrounding WM and CSF tissue, voxels with a GM

probability of <50% in the aging/AD template were removed from the warped AV45 scans. Finally, warped and masked AV45 scans were smoothed with a Gaussian smoothing kernel of 8-mm FWHM. Cortex-to-cerebellar GM SUVRs derived from the SPM-processed AV45-PET scans were highly consistent with the values reported on the ADNI server (correlation coefficient: $r = 0.98$).

2.6. Statistical analysis

Analyses were performed using the statistical software IBM SPSS Statistics (version 15). All statistical tests are two-tailed and statistical significance was set at $P < .05$. Group differences in demographics (Table 1) were analyzed using Fisher's exact test for categorical variables and group-wise t -tests for continuous variables.

2.6.1. Effects of diagnosis and amyloid status on BF and hippocampus volumes

The overall effects of diagnosis and amyloid status on volumes of the BF and the hippocampus were assessed using analysis of covariance (ANCOVA), controlling for age and gender. Pairwise follow-up tests for differences in the estimated marginal means of the respective volumes were evaluated for the diagnosis-specific contrasts of interest, EMCI(+) < CN(–), and LMCI(+) < CN(–), as well as for the amyloid-specific contrasts of interest, CN(+) < CN(–), EMCI(+) < EMCI(–), and LMCI(+) < LMCI(–). Reported P values for the pairwise group comparisons were not further corrected for multiple comparisons and should thus be considered exploratory.

2.6.2. Association between amyloid load and regional brain volume

Partial correlations between cortical AV45 SUVR and BF and hippocampus volumes, respectively, were assessed within amyloid-positive subjects, controlling for diagnosis (two dummy-coded covariates), age, gender, and $APOE \epsilon 4$

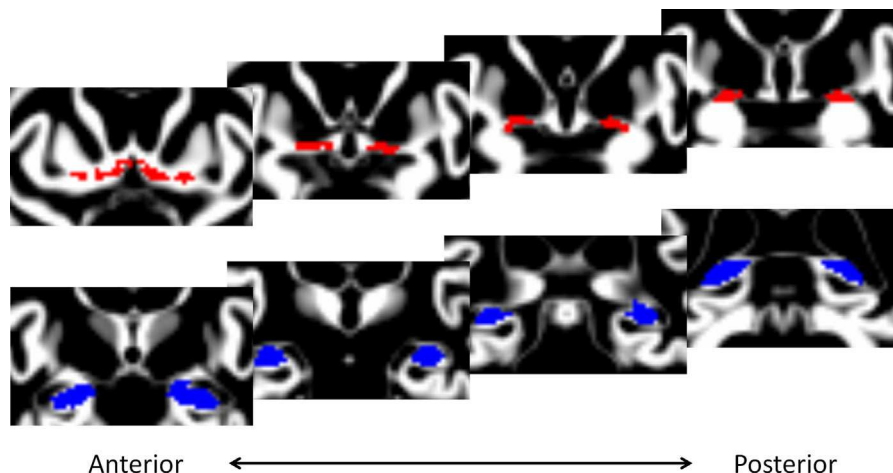


Fig. 1. Overview of the basal forebrain and hippocampus regions of interest. Basal forebrain (red) and hippocampus (blue) regions of interest (ROIs) are superimposed on representative coronal sections of the gray-matter partition of the aging/AD-specific template, magnified to better depict the respective ROIs.

Table 1
Subject demographics for amyloid-stratified diagnostic groups

	N	Age	Gender (F/M)	MMSE	APOE ε4- positive (%)
CN(–)	36	76.2 (SD 6.0)	18/18	29.1 (SD 1.1)	19.4%
CN(+)	21	77.6 (SD 5.6)	12/9	28.9 (SD 1.0)	42.9%
EMCI(–)	90	69.8 (SD 7.9)	49/41	28.7 (SD 1.3)	24.4%
EMCI(+)	66	73.1 (SD 6.9)*,§	39/27	27.8 (SD 1.7) ^{†,§}	57.6% ^{†,§}
LMCI(–)	9	74.0 (SD 10.9)	6/3	28.4 (SD 1.5)	33.3%
LMCI(+)	23	73.4 (SD 8.9)	12/11	26.9 (SD 2.0) ^{†,‡}	82.6% ^{†,‡}

Abbreviations: APOE ε4-positive, carrier of one or two APOE ε4 alleles; F, female; M, male; MMSE, Mini-Mental State Examination; SD, standard deviation.

NOTE. Diagnostic groups were dichotomized into amyloid-positive (+) and amyloid-negative (–) subgroups based on a cortex-to-cerebellar gray-matter AV45 standard uptake value ratio (SUVR) threshold of 1.28.

*Significantly different ($P < .05$) from the control group of amyloid-negative, healthy elderly subjects [CN(–)].

[†]Significantly different ($P < .01$) from the control group of amyloid-negative healthy elderly subjects [CN(–)].

[‡]Significantly different ($P < .05$) from amyloid-negative subjects of the same diagnostic category.

[§]Significantly different ($P < .01$) from amyloid-negative subjects of the same diagnostic category.

status (1 if at least one APOE ε4 allele is present, 0 otherwise). Additional correlation analyses were performed within each diagnostic group separately. Whereas the categorical comparison of BF volume between amyloid-stratified subgroups assessed associations between BF atrophy and presence of amyloid pathology, the complementary correlational analyses assessed specific associations between BF atrophy and cortical amyloid load within preclinical and prodementia stages of AD. Thus, amyloid-negative subjects were excluded from these analyses. Reported P values of the correlation analyses were not further corrected for multiple comparisons and should thus be considered exploratory.

To test for regional specificity of the association, SPM8 software was used to compute two separate voxel-based regression analyses across the CN(+) and EMCI(+) subgroups, which were the only groups that showed a significant correlation between BF volume and global cortical AV45 SUVR in the previous analysis. First, associations between BF volume and regional AV45 uptake were assessed by regressing BF volume on the SPM-processed AV45 scans. AV45 maps were proportionately scaled to mean AV45 uptake in cerebellar GM, and analysis was controlled for age, gender, APOE ε4 status, and diagnosis (binary coded). Based on the highly significant association between global cortical AV45 SUVR and volume of the BF ROI, voxelwise effects were assessed at a conservative statistical threshold of $P < .05$, corrected for multiple comparisons using the familywise error.

Effects of global amyloid load on regional GM volume throughout the whole brain were assessed in an exploratory way by regressing global cortical AV45

SUVR on the preprocessed GM maps, controlling for total intracranial volume (TIV), age, gender, APOE ε4 positivity, and diagnosis. These effects were assessed at an uncorrected threshold of $P < .001$ and a cluster extension threshold of 20 continuous voxels. In addition, a more lenient statistical threshold of $P < .005$, uncorrected, was applied to confirm the regional specificity of the findings.

3. Results

3.1. Amyloid deposition within diagnostic groups

Amyloid positivity was detected in 36.8% of CN subjects, 42.3% of EMCI subjects, and 71.9% of LMCI subjects. The percentage of amyloid-positive subjects was significantly higher in the LMCI group compared with both the CN ($P = .002$) and EMCI ($P = .003$) groups, but it did not differ significantly between the EMCI and CN groups. Table 1 summarizes the mean age, gender ratio, global neuropsychologic profile, and APOE ε4 frequencies of the amyloid-stratified subgroups.

3.2. Effects of diagnosis and amyloid status on BF and hippocampus volumes

Age- and gender-adjusted means of TIV-normalized BF and hippocampus volumes for each of the subgroups are presented in Table 2. There was a significant overall effect of group on BF ($F = 2.68$, $P = .02$) and hippocampus volume ($F = 3.63$, $P = .003$). When compared with the CN(–) control group, BF and hippocampus volumes showed significant reductions of 7.6% ($P = .02$) and 9.0% ($P < .001$), respectively, in the LMCI(+) group, but not in the EMCI(+) group.

Table 2
Group differences in basal forebrain and hippocampus volumes

	BF	Hippocampus
CN(–)	761 (730–793)	3622 (3510–3734)
CN(+)	771 (730–813)	3662 (3514–3809)
EMCI(–)	765 (745–785)	3545 (3473–3616)
EMCI(+)	730 (707–753) [†]	3523 (3441–3604)
LMCI(–)	723 (661–785)	3426 (3205–3647)
LMCI(+)	703 (664–742)*	3296 (3157–3434) [‡]

Abbreviation: TIV, total intracranial volume.

NOTE. Group means of age- and gender corrected TIV-normalized basal forebrain (BF) and hippocampus volumes (estimated marginal means). 95% confidence interval in parentheses. Diagnostic groups were dichotomized into amyloid-positive (+) and amyloid-negative (–) subgroups based on a cortex-to-cerebellar gray-matter AV45 standard uptake value ratio (SUVR) threshold of 1.28.

*Significantly different ($P < .05$) from the control group of amyloid-negative, healthy elderly subjects [CN(–)].

[†]Significantly different ($P < .05$) from amyloid-negative subjects of the same diagnostic category.

[‡]Significantly different ($P < .01$) from the control group of amyloid-negative, healthy elderly subjects [CN(2)].

Regarding the amyloid-specific contrasts, BF volume was significantly reduced in EMCI(+) compared with EMCI(−) ($P = .02$), but not in CN(+) or LMCI(+), when compared with their respective amyloid-negative subgroups (Table 2). Hippocampus volume did not differ between amyloid-positive and -negative subgroups within any diagnostic group.

3.3. Association between BF volume and cortical amyloid load

Cortical AV45 SUVR was significantly associated with normalized BF volume ($r_{\text{part}} = -0.32$, $P < .001$), but not hippocampus volume ($r_{\text{part}} = -0.06$, $P > .1$), across amyloid-positive subjects, when controlling for diagnosis, age, gender, and *APOE* $\epsilon 4$ status. Fig. 2 plots normalized BF and hippocampus volume against cortical AV45 SUVR in amyloid-positive subjects separately for each diagnostic group. Significant correlations between BF volume and cortical AV45 SUVR were found in CN(+) ($r = -0.45$, $P = .04$) and EMCI(+) ($r = -0.45$, $P < .001$), but not in LMCI(+) groups. These correlations also remained significant when controlling for age, gender, and *APOE* $\epsilon 4$ status [CN(+): $r_{\text{part}} = -0.57$, $P = .01$; EMCI(+): $r_{\text{part}} = -0.33$, $P = .008$]. In contrast, no significant association between cortical amyloid load and hippocampus atrophy could be detected in any subgroup.

Results from the voxel-based regression of cortical AV45 SUVR on preprocessed GM maps across the CN(+) and EMCI(+) groups are illustrated in Fig. 3. Confirming findings from the ROI-based analysis, unbiased voxel-based analysis revealed a large bilateral cluster in the basal forebrain, covering most parts of the BF ROI [16], particularly the NBM. The BF clusters also covered the center-of-gravity coordinates for nuclei Ch3, Ch4, and Ch4p, as derived from probabilistic cytoarchitectonic maps [21]. Interestingly, subcortical GM structures bordering the cholinergic BF were largely spared, although the BF cluster extended anteriorly into the ventral striatum and posteriorly into the putamen and dorsal amygdala. Most of the effects in the cholinergic BF also survived the statistical threshold of $P < .001$, uncorrected, especially in the right hemisphere. Cortical clusters were detected in the dorso- and ventromedial prefrontal cortex, ventral precuneus/retrosplenial cortex, bilateral middle frontal gyri, and bilateral temporoparietal junction.

Results from the voxel-based regression of BF volume on preprocessed AV45 maps are illustrated in Fig. 4. Significant inverse associations between BF volume and regional AV45 SUVR were detected in several cortical paralimbic and heteromodal association areas, including the bilateral precuneus/posterior cingulate, dorso- and ventromedial prefrontal cortex, anterior cingulate, inferior and middle temporal gyri, and the right temporoparietal junction. In addition, one subcortical cluster was detected

corresponding to the left putamen, but no effects were seen within the BF proper.

4. Discussion

In this study we have reported the first in vivo evidence of an association between BF atrophy and elevated cortical amyloid load in preclinical and prodementia stages of AD, as defined by PET-evidenced amyloid pathology in addition to cognitive criteria [25]. Given that the BF houses the cortically projecting cholinergic cells known to be particularly vulnerable to age- and AD-related neurodegeneration [26], this in vivo association is likely to reflect findings from several human autopsy studies showing associations between amyloid pathology and cholinergic atrophy in AD [4,10–12]. Interestingly, associations between amyloid plaque load, cortical ChAT activity, and cholinergic fiber loss have also been found in postmortem brain tissue of elderly individuals who exhibited significant amyloid pathology but had died without a history of neurologic disease or cognitive loss prior to death [13,14].

Cross-sectional associations between PET-measured amyloid load and MRI-derived measures of brain atrophy have been examined in earlier studies, both using correlational approaches as well as bivariate comparisons between amyloid-positive and -negative subgroups [27–31], but none of these studies explicitly addressed BF volumes. Interestingly, in one study a voxelwise regression of global amyloid load on preprocessed GM maps was used, analogous to the approach employed in the present study, and very similar regional effects were found in a group of healthy elderly subjects with subjective cognitive complaints, but not in subjects with MCI or clinically manifest AD [29]. Besides similar neocortical effects, that study also reported a distinct subcortical cluster that clearly overlaps with the NBM. However, in the study by Chetelat et al. [29], this cluster further included large parts of the amygdala and the head of the hippocampus, and no reference to the cholinergic system of the BF was made.

The missing association in advanced stages of MCI may be explained by the amyloid-cascade theory, which states that amyloid pathology is only indirectly linked to measurable atrophy through the induction of downstream pathologic events, such as the formation of intracellular neurofibrillary tangles. Consequently, associations between amyloid deposition and brain atrophy may be more likely to occur in very early and probably pre-symptomatic stages of the disease process, whereas ongoing atrophy in symptomatic and clinically manifest stages of the disease may be governed by neurofibrillary processes in the face of saturating cerebral amyloid deposition [32,33].

Surprisingly, despite the relatively strong negative association between amyloid load and BF volume in amyloid-positive cognitively normal individuals, mean BF volume of this group was not significantly smaller compared with

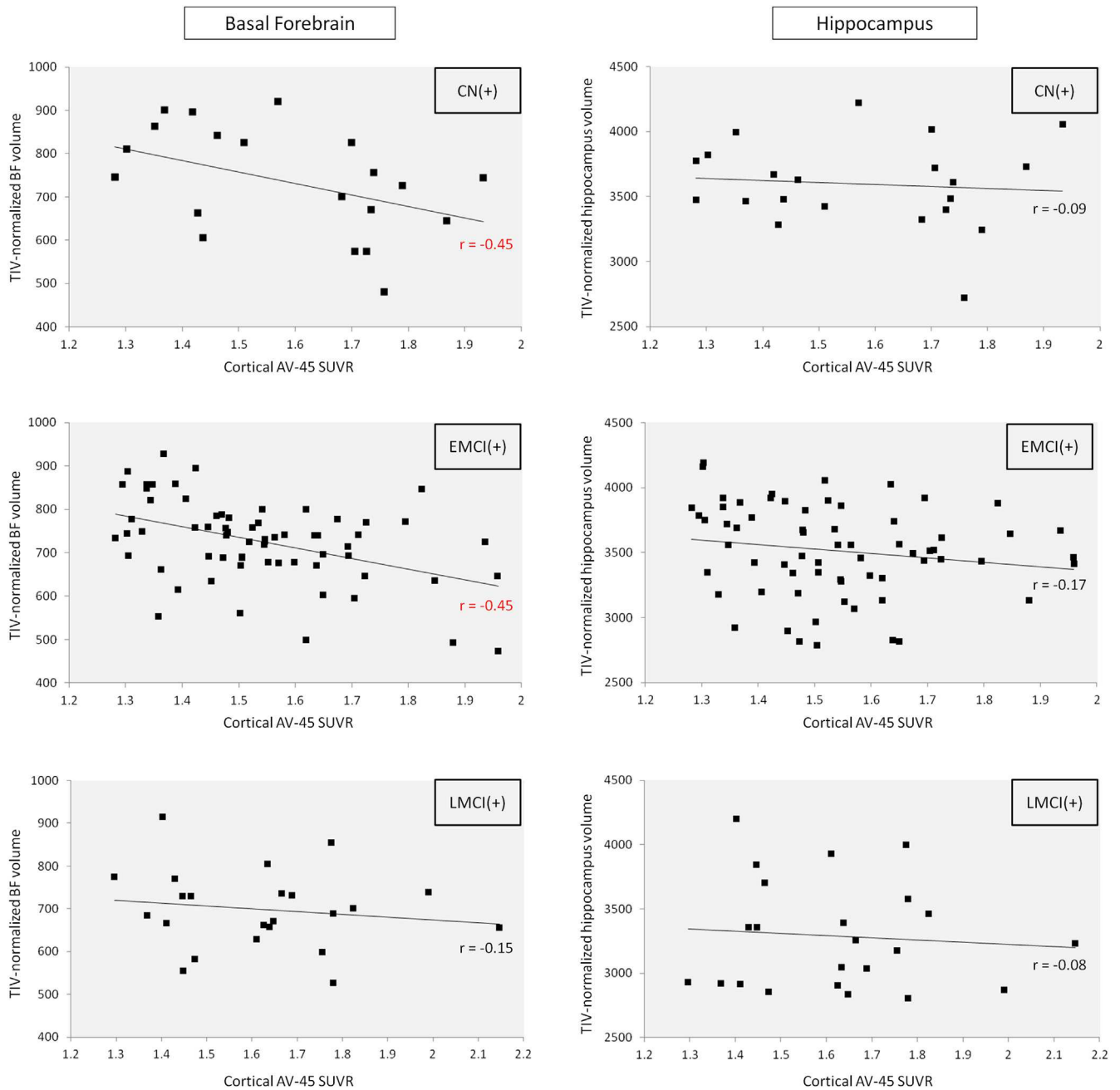


Fig. 2. Basal forebrain and hippocampus volume in relation to global cortical amyloid load TIV-normalized basal forebrain (left column) and hippocampus volume (right column) are plotted against cortex-to-cerebellar gray-matter AV45 standard uptake value ratios (SUVR) in amyloid-positive subjects (≥ 1.28 cortical AV45 SUVR), separately for each diagnostic group. Black line indicates linear regression trend. Red: statistical significance at $P < .05$; r , Pearson's correlation coefficient; TIV, total intracranial volume.

the amyloid-negative control group. This may be due to an overrepresentation of individuals with large brain volumes in amyloid-positive, healthy individuals, allowing these subjects to maintain normal cognition in the face of considerable brain pathology [34].

Although cross-sectional correlational studies do not allow for inference on the directionality of the effects, the observed associations between amyloid deposition and brain atrophy are usually interpreted as reflecting neurotoxic ef-

fects of the amyloid aggregates. In this regard, the higher correlation between amyloid load and BF volume compared with hippocampus volume observed here may reflect a reportedly high vulnerability of BF cholinergic cells to amyloid-induced neurodegeneration [35,36]. Accordingly, in postmortem brain tissue of AD patients, amyloid deposits within the BF were found to be entirely restricted to the cholinergic cell clusters and correlated with neuronal loss [37].

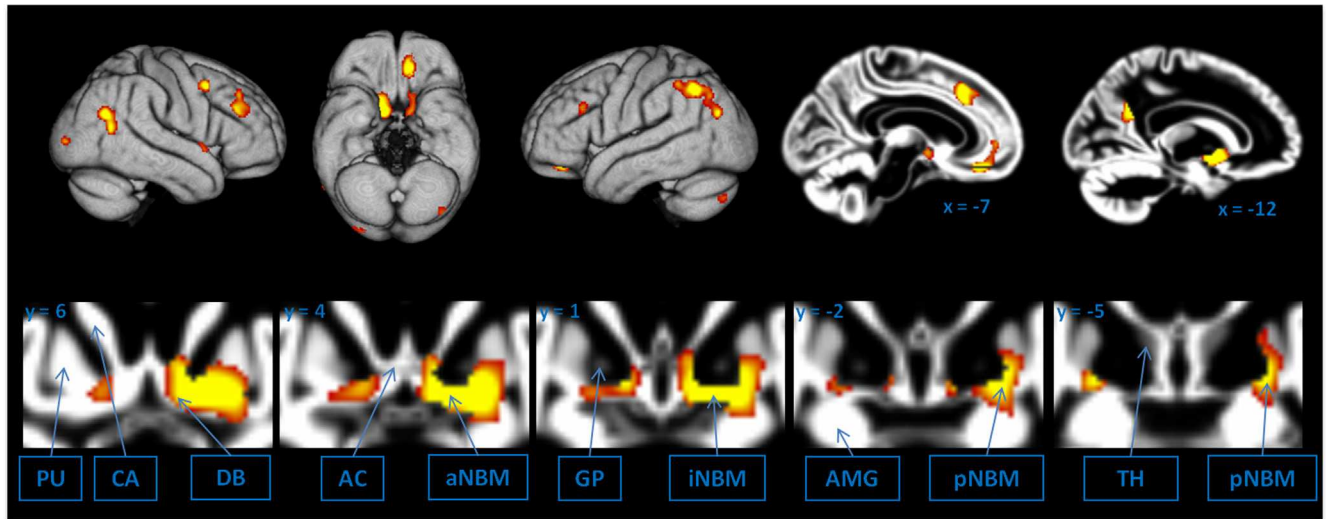


Fig. 3. Effects of global cortical amyloid load on regional gray-matter atrophy. Voxel-wise multiple linear regression of global cortical AV45 SUVR on pre-processed gray-matter maps within combined CN(+) and EMCI(+) subgroups. Analysis was controlled for TIV, age, gender, *APOE* ϵ 4 status, and diagnosis. Statistical significance is color-coded from yellow ($P < .001$, uncorrected) to red ($P < .005$, uncorrected). Cluster extension threshold was set to a minimum of 20 continuous voxels. Top row: Effects superposed on rendered views of the right, ventral, and left brain surfaces, as well as on two sagittal sections of the reference template. Bottom row: Effects superposed on coronal sections of the reference template, magnified to better depict the basal forebrain ROI. Blue arrows: Locations of basal forebrain cholinergic nuclei as well as external landmarks for better anatomic orientation. Blue numbers: Approximate levels of orthogonal sections in MNI space, based on a high-dimensional coordinate transformation from the aging/AD-specific reference space of this study to the MNI152 standard template. AC, anterior commissure; AMG, amygdala; DB, diagonal band of Broca; CA, caudate; GP, globus pallidus; (a, i, p) NBM, anterior, intermediate, posterior nucleus basalis Meynert; PU, putamen; TH, thalamus.

In the case of the cholinergic BF, however, the observed correlation with cortical amyloid load may also be interpreted in the other direction, given that there is considerable experimental evidence that cholinergic degeneration may contribute to increased cortical amyloid deposition due to reduced cholinergic signaling (as reviewed by Schliebs and Arendt [7]). Thus, *in vitro* as well as *in vivo* studies on animal models have shown that cholinergic receptor activation favors the non-amyloidogenic route of cortical APP processing [38,39]. Accordingly, experimental lesions to the

cholinergic BF in wild-type animals led to increased amyloid deposition with age [9,40,41].

The sequence of the underlying pathogenetic events cannot be derived from our data. However, the association between BF atrophy and amyloid accumulation could be either local in the BF or mediated via distant cortical projections. The voxel-based regression of BF volume on AV45 maps in this study revealed associations in widespread areas of paralimbic and heteromodal association cortices, which are known to receive dense cholinergic innervation [42],

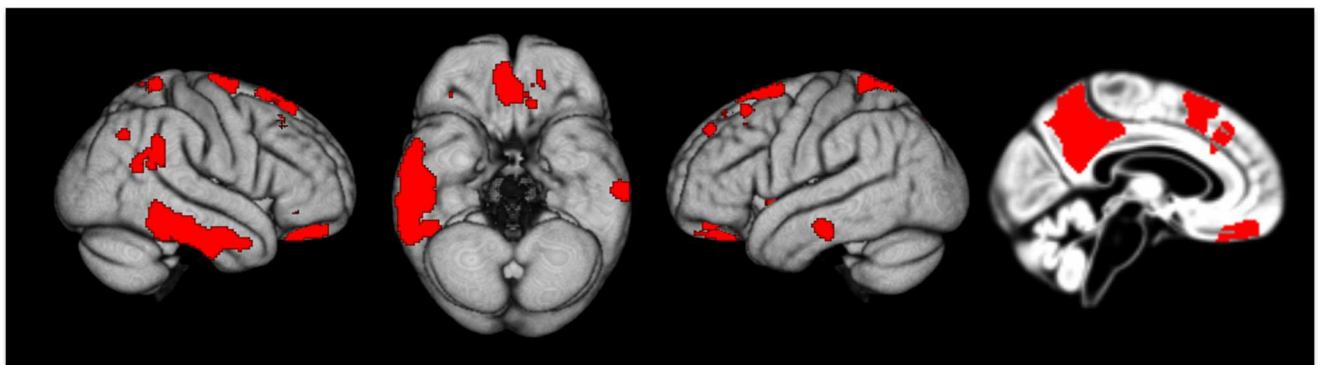


Fig. 4. Effects of basal forebrain atrophy on regional amyloid deposition. Voxelwise multiple linear regression of TIV normalized basal forebrain (BF) volume on preprocessed AV45 maps within combined CN(+) and EMCI(+) subgroups. AV45 maps were proportionately scaled to cerebellar AV45 uptake to obtain voxelwise standard uptake value ratios (SUVR). Analysis was controlled for age, gender, *APOE* ϵ 4 status, and diagnosis. Statistical threshold was set to $P < .05$, corrected for multiple comparisons using the familywise error. Associations between BF volume and regional AV45 uptake are superimposed on rendered views of the right, ventral, and left brain surfaces as well as a midsagittal section of the reference template. TIV, total intracranial volume.

but no local effects within the BF were observed. Hence, these findings suggest a distant rather than a local effect of the interaction between amyloid load and BF atrophy in our data. Due to the very small size of BF structures compared with the resolution of PET images, these negative findings must be interpreted with caution. However, they coincide with postmortem evidence that amyloid deposition in the cholinergic BF does not occur before relatively advanced stages of amyloid pathology [43]. Alternatively, the cortically projecting cholinergic neurons of the BF may degenerate in a retrograde fashion due to neurotoxicity of amyloid deposits in their cortical target areas. Such a model is supported by transgenic animal models of altered APP metabolism and increased amyloid deposition. These animals showed a selective degeneration of cortical cholinergic fiber terminals in proximity to amyloid plaques as well as reduced volumes but preserved numbers of BF cholinergic neurons compared with wild-type animals [8,44]. On the other hand, and with respect to evidence for cholinergic modulation of amyloidogenic APP processing, decreased cholinergic signaling from a degenerating BF cholinergic system would be expected to have a stronger effect on amyloid deposition in cortical projection sites compared with local deposition in the BF.

Our study has several limitations. First, the results may depend partly on the selection of the threshold for amyloid classification. The AV45 PET threshold used in our study corresponds to a previously established Pittsburgh compound B PET threshold SUVR of 1.47 [24]. We repeated the main analyses using two alternative thresholds, which have been found in a recent neuropathologic study to correspond to first signs of amyloid accumulation or pathologically relevant amyloid accumulation, respectively [15]. Results were not significantly altered by the choice of classification threshold, with the exception being the comparison of BF volume between EMCI(+) and EMCI(–), which reached only trend-level significance at the lowest threshold.

A further limitation of our study is that the employed *in vivo* marker of BF atrophy is necessarily an indirect marker of cholinergic degeneration, given that cholinergic cells cannot be distinguished directly on current MRI contrasts. The marker measures GM volume in a BF ROI that has been informed by histologic mapping of the forebrain's cholinergic nuclei [16]. Recently, the cytoarchitectonic mapping of the cholinergic nuclei into MRI standard space was further refined by pooling information from a sample of 10 healthy subjects [21]. To ensure that our findings did not critically depend on the definition of the cholinergic space in the employed BF ROI, we additionally conducted an unbiased voxel-based analysis. This analysis showed distinct bilateral clusters in the BF that overlapped considerably with the cholinergic space defined by our BF ROI as well as with the NBM coordinates reported by Zaborszky and colleagues [21]. The use of cytoarchitectonic reference maps increases confidence in addressing the cholinergic space of the BF

compared with simpler measurements of the substantia innominata centered on the anterior commissure [45,46]. However, due to the indirect character of the measurement, it cannot be excluded that differences in volume may also reflect changes in other neuronal or glial components of the BF.

Acknowledgments

This work was supported by grants from the Interdisciplinary Faculty, Department “Individual and Societal Ageing,” University of Rostock (to S.J.T.). Data collection and sharing for this project was funded by the Alzheimer's Disease Neuroimaging Initiative (ADNI) (National Institutes of Health Grant U01 AG024904). The ADNI was launched in 2003 by the National Institute on Aging (NIA), the National Institute of Biomedical Imaging and Bioengineering (NIBIB), the U.S. Food and Drug Administration (FDA), private pharmaceutical companies, and nonprofit organizations, as a \$60 million, 5-year public–private partnership. The Principal Investigator of this initiative is Michael W. Weiner, MD, VA Medical Center, and University of California–San Francisco. The ADNI is the result of the efforts of many coinvestigators from a broad range of academic institutions and private corporations, and subjects have been recruited from over 50 sites across the USA and Canada. The ADNI is funded by the National Institute on Aging, the National Institute of Biomedical Imaging and Bioengineering, and through generous contributions from the following companies: Abbott; the Alzheimer's Association; the Alzheimer's Drug Discovery Foundation; Amorfix Life Sciences, Ltd.; AstraZeneca; Bayer HealthCare; BioClinica, Inc.; Biogen Idec, Inc.; Bristol-Myers Squibb Co.; Eisai, Inc.; Elan Pharmaceuticals, Inc.; Eli Lilly and Co.; F. Hoffmann-La Roche, Ltd., and its affiliated company Genentech, Inc.; GE Healthcare; Innogenetics, N.V.; IXICO, Ltd.; Janssen Alzheimer Immunotherapy Research & Development, LLC; Johnson & Johnson Pharmaceutical Research & Development LLC; Medpace, Inc.; Merck & Co., Inc.; Meso Scale Diagnostics, LLC.; Novartis Pharmaceuticals Corp.; Pfizer Inc.; Servier; Synarc, Inc.; and the Takeda Pharmaceutical Co. The Canadian Institutes of Health Research provides funds to support ADNI clinical sites in Canada. Private Rev November 7, 2012 sector contributions are facilitated by the Foundation for the National Institutes of Health (www.fnih.org). The grantee organization is the Northern California Institute for Research and Education, and the study is coordinated by the Alzheimer's Disease Cooperative Study at the University of California, San Diego. ADNI data are disseminated by the Laboratory for Neuro Imaging at the University of California, Los Angeles. This research was also supported by NIH grants (P30 AG010129 and K01 AG030514).

This study was presented in part and published as an oral presentation at the Alzheimer's Association International

Conference on Alzheimer's Disease (AAICAD), July 14–19, 2012, Vancouver, BC, Canada.

RESEARCH IN CONTEXT

1. Systematic review: We searched the PubMed database for studies examining the relationship between amyloid pathology and cholinergic atrophy in vivo, using combinations of the following search terms: amyloid; PET; MRI; atrophy; cholinergic; basal forebrain; nucleus basalis Meynert; and substantia innominata. Several recent studies assessed AD-related changes in MRI-based measurements of the basal forebrain/substantia innominata as in vivo proxies for cholinergic atrophy, but none of these studies examined relations to in vivo-measured amyloid pathology. Although several studies were found that assessed associations between PET-measured amyloid deposition and regional atrophy on MRI, none explicitly examined volumes of the BF or parts thereof.
2. Interpretation: The in vivo correlations between PET-measured amyloid load and MRI-derived volumes of the BF likely reflect the distinct association between amyloid pathology and cholinergic degeneration as reported previously in human autopsy studies and experimental animal models.
3. Future directions: Further studies are needed to determine the neuropathologic underpinnings of amyloid-related changes in MRI-derived BF volumes and their relation to cortical cholinergic function.

References

- [1] Mesulam MM, Mufson EJ, Levey AI, Wainer BH. Cholinergic innervation of cortex by the basal forebrain: cytochemistry and cortical connections of the septal area, diagonal band nuclei, nucleus basalis (substantia innominata), and hypothalamus in the rhesus monkey. *J Comp Neurol* 1983;214:170–97.
- [2] Mann DM, Yates PO, Marcyniuk B. Changes in nerve cells of the nucleus basalis of Meynert in Alzheimer's disease and their relationship to ageing and to the accumulation of lipofuscin pigment. *Mech Ageing Dev* 1984;25:189–204.
- [3] Whitehouse PJ, Price DL, Clark AW, Coyle JT, DeLong MR. Alzheimer disease: evidence for selective loss of cholinergic neurons in the nucleus basalis. *Ann Neurol* 1981;10:122–6.
- [4] Perry EK, Tomlinson BE, Blessed G, Bergmann K, Gibson PH, Perry RH. Correlation of cholinergic abnormalities with senile plaques and mental test scores in senile dementia. *BMJ* 1978;2:1457–9.
- [5] Bartus RT, Dean RL 3rd, Beer B, Lippa AS. The cholinergic hypothesis of geriatric memory dysfunction. *Science* 1982;217:408–14.
- [6] Hardy J, Selkoe DJ. The amyloid hypothesis of Alzheimer's disease: progress and problems on the road to therapeutics. *Science* 2002;297:353–6.
- [7] Schliebs R, Arendt T. The significance of the cholinergic system in the brain during aging and in Alzheimer's disease. *J Neural Transm* 2006;113:1625–44.
- [8] Boncristiano S, Calhoun ME, Kelly PH, Pfeifer M, Bondolfi L, Stalder M, et al. Cholinergic changes in the APP23 transgenic mouse model of cerebral amyloidosis. *J Neurosci* 2002;22:3234–43.
- [9] Beach TG. Physiologic origins of age-related beta-amyloid deposition. *Neurodegen Dis* 2008;5:143–5.
- [10] Beach TG, McGeer EG. Senile plaques, amyloid beta-protein, and acetylcholinesterase fibres: laminar distributions in Alzheimer's disease striate cortex. *Acta Neuropathol* 1992;83:292–9.
- [11] Arendt T, Bigl V, Tennstedt A, Arendt A. Neuronal loss in different parts of the nucleus basalis is related to neuritic plaque formation in cortical target areas in Alzheimer's disease. *Neuroscience* 1985;14:1–14.
- [12] Ikonovic MD, Klunk WE, Abrahamson EE, Wu J, Mathis CA, Scheff SW, et al. Precuneus amyloid burden is associated with reduced cholinergic activity in Alzheimer disease. *Neurology* 2011;77:39–47.
- [13] Beach TG, Honer WG, Hughes LH. Cholinergic fibre loss associated with diffuse plaques in the non-demented elderly: the preclinical stage of Alzheimer's disease? *Acta Neuropathol* 1997;93:146–53.
- [14] Potter PE, Rauschkolb PK, Pandya Y, Sue LI, Sabbagh MN, Walker DG, et al. Pre- and post-synaptic cortical cholinergic deficits are proportional to amyloid plaque presence and density at preclinical stages of Alzheimer's disease. *Acta Neuropathol* 2011;122:49–60.
- [15] Fleisher AS, Chen K, Liu X, Roontiva A, Thiyyagura P, Ayutyanont N, et al. Using positron emission tomography and florbetapir F18 to image cortical amyloid in patients with mild cognitive impairment or dementia due to Alzheimer disease. *Arch Neurol* 2011;68:1404–11.
- [16] Teipel SJ, Flatz WH, Heinsen H, Bokde AL, Schoenberg SO, Stockel S, et al. Measurement of basal forebrain atrophy in Alzheimer's disease using MRI. *Brain* 2005;128:2626–44.
- [17] Grothe M, Heinsen H, Teipel SJ. Atrophy of the cholinergic basal forebrain over the adult age range and in early stages of Alzheimer's disease. *Biol Psychiatry* 2013;71:805–13.
- [18] Grothe M, Heinsen H, Teipel S. Longitudinal measures of cholinergic forebrain atrophy in the transition from healthy aging to Alzheimer's disease. *Neurobiol Aging* 2012;34:1210–20.
- [19] Grothe M, Zaborszky L, Atienza M, Gil-Neciga E, Rodriguez-Romero R, Teipel SJ, et al. Reduction of basal forebrain cholinergic system parallels cognitive impairment in patients at high risk of developing Alzheimer's disease. *Cereb Cortex* 2010;20:1685–95.
- [20] Ashburner J. A fast diffeomorphic image registration algorithm. *Neuroimage* 2007;38:95–113.
- [21] Zaborszky L, Hoemke L, Mohlberg H, Schleicher A, Amunts K, Zilles K. Stereotaxic probabilistic maps of the magnocellular cell groups in human basal forebrain. *Neuroimage* 2008;42:1127–41.
- [22] Teipel SJ, Grothe M, Lista S, Toschi N, Garaci FG, Hampel H. Relevance of magnetic resonance imaging for early detection and diagnosis of Alzheimer disease. *Med Clin N Am* 2013;97:399–424.
- [23] Pruessner JC, Li LM, Serles W, Pruessner M, Collins DL, Kabani N, et al. Volumetry of hippocampus and amygdala with high-resolution MRI and three-dimensional analysis software: minimizing the discrepancies between laboratories. *Cereb Cortex* 2000;10:433–42.
- [24] Landau SM, Breault C, Joshi AD, Pontecorvo M, Mathis CA, Jagust WJ, et al. Amyloid-beta imaging with Pittsburgh compound B and florbetapir: comparing radiotracers and quantification methods. *J Nucl Med* 2013;54:70–7.
- [25] Jack CR Jr, Albert MS, Knopman DS, McKhann GM, Sperling RA, Carrillo MC, et al. Introduction to the recommendations from the National Institute on Aging–Alzheimer's Association workgroups on diagnostic guidelines for Alzheimer's disease. *Alzheimers Dement* 2011;7:257–62.

- [26] Mesulam M, Shaw P, Mash D, Weintraub S. Cholinergic nucleus basalis tauopathy emerges early in the aging-MCI-AD continuum. *Ann Neurol* 2004;55:815–28.
- [27] Mormino EC, Kluth JT, Madison CM, Rabinovici GD, Baker SL, Miller BL, et al. Episodic memory loss is related to hippocampal-mediated beta-amyloid deposition in elderly subjects. *Brain* 2009;132:1310–23.
- [28] Storandt M, Mintun MA, Head D, Morris JC. Cognitive decline and brain volume loss as signatures of cerebral amyloid-beta peptide deposition identified with Pittsburgh compound B: cognitive decline associated with Abeta deposition. *Arch Neurol* 2009;66:1476–81.
- [29] Chetelat G, Villemagne VL, Bourgeat P, Pike KE, Jones G, Ames D, et al. Relationship between atrophy and beta-amyloid deposition in Alzheimer disease. *Ann Neurol* 2010;67:317–24.
- [30] Becker JA, Hedden T, Carmasin J, Maye J, Rentz DM, Putcha D, et al. Amyloid-beta associated cortical thinning in clinically normal elderly. *Ann Neurol* 2011;69:1032–42.
- [31] Drzezga A, Becker JA, van Dijk KR, Sreenivasan A, Talukdar T, Sullivan C, et al. Neuronal dysfunction and disconnection of cortical hubs in non-demented subjects with elevated amyloid burden. *Brain* 2011;134:1635–46.
- [32] Jack CR Jr, Knopman DS, Jagust WJ, Shaw LM, Aisen PS, Weiner MW, et al. Hypothetical model of dynamic biomarkers of the Alzheimer's pathological cascade. *Lancet Neurol* 2010;9:119–28.
- [33] Buchhave P, Minthon L, Zetterberg H, Wallin AK, Blennow K, Hansson O. Cerebrospinal fluid levels of beta-amyloid 1–42, but not of tau, are fully changed already 5 to 10 years before the onset of Alzheimer dementia. *Arch Gen Psychiatry* 2012;69:98–106.
- [34] Chetelat G, Villemagne VL, Pike KE, Baron JC, Bourgeat P, Jones G, et al. Larger temporal volume in elderly with high versus low beta-amyloid deposition. *Brain* 2010;133:3349–58.
- [35] Zheng WH, Bastianetto S, Mennicken F, Ma W, Kar S. Amyloid beta peptide induces tau phosphorylation and loss of cholinergic neurons in rat primary septal cultures. *Neuroscience* 2002;115:201–11.
- [36] Harkany T, de Jong GI, Soos K, Penke B, Luiten PG, Gulya K. Beta-amyloid (1–42) affects cholinergic but not parvalbumin-containing neurons in the septal complex of the rat. *Brain Res* 1995;698:270–4.
- [37] Arendt T, Taubert G, Bigl V, Arendt A. Amyloid deposition in the nucleus basalis of Meynert complex: a topographic marker for degenerating cell clusters in Alzheimer's disease. *Acta Neuropathol* 1988;75:226–32.
- [38] Bailey JA, Ray B, Greig NH, Lahiri DK. Rivastigmine lowers Abeta and increases sAPPalpha levels, which parallel elevated synaptic markers and metabolic activity in degenerating primary rat neurons. *PLoS One* 2011;6:e21954.
- [39] Lahiri DK, Utsuki T, Chen D, Farlow MR, Shoaib M, Ingram DK, et al. Nicotine reduces the secretion of Alzheimer's beta-amyloid precursor protein containing beta-amyloid peptide in the rat without altering synaptic proteins. *Ann NY Acad Sci* 2002;965:364–72.
- [40] Arendash GW, Millard WJ, Dunn AJ, Meyer EM. Long-term neuropathological and neurochemical effects of nucleus basalis lesions in the rat. *Science* 1987;238:952–6.
- [41] Aztiria E, Cataudella T, Spampinato S, Leanza G. Septal grafts restore cognitive abilities and amyloid precursor protein metabolism. *Neurobiol Aging* 2009;30:1614–25.
- [42] Mesulam MM, Geula C. Chemoarchitectonics of axonal and perikaryal acetylcholinesterase along information processing systems of the human cerebral cortex. *Brain Res Bull* 1994;33:137–53.
- [43] Thal DR, Rub U, Orantes M, Braak H. Phases of A beta-deposition in the human brain and its relevance for the development of AD. *Neurology* 2002;58:1791–800.
- [44] Bell KF, Ducatenzeiler A, Ribeiro-da-Silva A, Duff K, Bennett DA, Cuello AC. The amyloid pathology progresses in a neurotransmitter-specific manner. *Neurobiol Aging* 2006;27:1644–57.
- [45] Hanyu H, Asano T, Sakurai H, Tanaka Y, Takasaki M, Abe K. MR analysis of the substantia innominata in normal aging, Alzheimer disease, and other types of dementia. *AJNR Am J Neuroradiol* 2002;23:27–32.
- [46] George S, Mufson EJ, Leurgans S, Shah RC, Ferrari C, deToledo-Morrell L. MRI-based volumetric measurement of the substantia innominata in amnesic MCI and mild AD. *Neurobiol Aging* 2011;32:1756–64.